06,13

Structure, dielectric and ferroelectric properties of $Ba_2NdFeNb_4O_{15}$ multiferroic thin films

© A.V. Pavlenko[1,2], T.S. Ilina[1,3], D.A. Kiselev[3], D.V. Stryukov[1], M.V. Ochkurov[2]

[1] Southern Scientific Center, Russian Academy of Sciences,
Rostov-on-Don, Russia
[2] Scientific Research Institute of Physics, Southern Federal University,
Rostov-on-Don, Russia
[3] National University of Science and Technology MISiS,
Moscow, Russia

E-mail: Antvpr@mail.ru

Received February 9, 2022
Revised February 9, 2022
Accepted February 16, 2022

The phase composition, nanostructure, and properties of $Ba_2NdFeNb_4O_{15}$ multiferroic thin films are studied by X-ray diffraction, dielectric spectroscopy, methods for analyzing ferroelectric properties, and scanning probe microscopy. Films were grown on the single-crystal Pt/MgO(001) substrate by a one-stage RF cathode sputtering technique in an oxygen atmosphere. It has been established that the $Ba_2NdFeNb_4O_{15}$ films are single-phase, impurity-free, and c-oriented, which made it possible to study their dielectric properties along the polar direction. tensile deformation of the unit cell (1.35% along the polar axis) has found in the films, which led to the realization of the ferroelectric phase in the BNFNO film at room temperature. The revealed dependencies and the prospects for using this material in the nanosized thin films form are discussed.

Keywords: multiferroic, dielectric characteristics, ferroelectric, tetragonal tungsten bronze.

DOI: 10.21883/PSS.2022.06.53827.286

1. Introduction

Presently, an intense study is under way for nonlinear dielectrics of a tetragonal tungsten bronze (TTB) structure with the general chemical formula $(A1)_2(A2)_4(C)_4(B1)_2(B2)_8O_{30}$ [1], which include $Ba_2LnFeNb_4O_{15}$ multiferroics (Ln — a rare earth element) [2–4]. Since 2009, the studies of the $Ba_2LnFeNb_4O_{15}$ ceramics had shown that they could be a base for creating new multiferroic structures, which combine ferroelectric and magnetic properties at the room temperature [2]. Then, these structures had been obtained as nanosized, which allowed considering their application in the function electronics and touch technology [5]. The crystal lattice of the $Ba_2LnFeNb_4O_{15}$ compounds is made of oxygen octahedrons, whose centers are statistically occupied with cations Fe^{3+} and Nb^{5+}, which form three-, four- and five-angle channels therebetween. The ions Ba^{2+} occupy the five-angle channels, the rare earth elements occupy the four-angle channels, while the three-angle ones are empty [6]. Unlike barium–strontium niobates, which are the best known materials with the TTB structure [1], the crystal structure of $Ba_2LnFeNb_4O_{15}$ is occupied [6,7]. However, there are vacancies in Ln positions during synthesis of the ceramics and single crystals, thereby largely affecting dielectric properties and a phase composition of the materials [6].

For the synthesis of thin films of complex oxides, various single- and multi-stage methods are used, while oxygen and argon are predominantly used as working gases [8,9]. One important method thereof is a single-stage method of gas-discharge HF-sputtering in an oxygen atmosphere [9], which allows fabricating films of complex oxides of various structural perfection, including ones with the TTB structure [10,11]. By using this method, we could produce polycrystalline, textured and single-crystal thin films of $Sr_{0.5}Ba_{0.5}Nb_2O_6$ [11] and $Sr_{0.61}Ba_{0.39}Nb_2O_6$ [10], as well as two-layer structures based thereon in combination with $(Ba,Sr)TiO_3$ [12] and $BiFeO_3$ [13]. Taking into account that a structure frame and parameters of a lattice cell for $Ba_2LnFeNb_4O_{15}$ and $S_xBa_{1-x}Nb_2O_6$ are sufficiently close (for example, for $Sr_{0.5}Ba_{0.5}Nb_2O_6$ $a = 12.46$ Å, $c = 3.944$ Å; for $Ba_2LnFeNb_4O_{15}$ — $a = 12.477$ Å, $c = 3.923$ Å), from our point of view this method can be efficiently used for producing various heterostructures with involvement of $Ba_2LnFeNb_4O_{15}$, too. By now, the scientific literature gives information on the synthesis of the $Ba_2LnFeNb_4O_{15}$ nanosized films on the Si, $SrTiO_3$ and MgO(001) substrates by the PLD method [2] and the magnetron sputtering method [3]. However, there is always an impurity of barium hexaferrite recorded in them. In this paper, we provide results of the first studies of the phase composition, a nanostructure, dielectric and ferroelectric properties of the $Ba_2NdFeNb_4O_{15}$ (BNFNO) thin films, which are grown by the gas-discharge HF-sputtering method.

2. Methods of production and research of samples

The gas-discharge HF-sputtering of the $Ba_2NdFeNb_4O_{15}$ films to the MgO (001) single-crystal substrate with a pre-deposited layer Pt was done by the unit „Plasma-50-SE". The initial temperature of the substrate — $\sim 400^\circ$C, the oxygen pressure in the chamber — 67 Pa, input HF-power — 150 W. A ceramic target of the stoichiometric composition of $Ba_2NdFeNb_4O_{15}$ was fabricated in the Department of Smart Materials and Nanotechnologies of Scientific Research Institute of Physics of Southern Federal University.

The phase composition, structural perfection of the films, the parameters of the lattice cell and orientation relationships between the film and the substrate were determined by radiography using the multi-function X-ray unit „RICOR" ($Cu_{K\alpha}$-radiation).

The topography, the domain structure, local switching processes and a signal relaxation of polarized areas of the films were obtained on the scanning probe microscopes Ntegra Prima (NT-MDT SI, Russia) and MFP-3D (Asylum Research, USA) in the modes of piezoresponse force microscopy (PFM) and Kelvin-mode (KM) using cantilevers NSG10/TiN (TipsNano) and NSG01/Pt (TipsNano), respectively. The images were processed and analyzed in the software applications Gwyddion (version 2.60) and WSxM.

The frequency dependences on the relative permittivity ($\varepsilon/\varepsilon_0$) and the dielectric loss tangent ($\mathrm{tg}\,\delta$) within the frequency range $f = 200-10^6$ Hz were obtained by means of the measurement bench based on the Agilent 4980A LCR-meter. The volt-Coulomb $P(U)$ characteristics were measured at $T = 25^\circ$C at the TFAnalyzer2000 analyzer. For positive and negative loop branches, the Hysteresis Software application calculated values of residual polarization (P_r^+ and P_r^-), maximum polarization ($P_{\max}^+$ and $P_{\max}^-$), the coercive field (E_c^+ and E_c^-), switching losses (W_{loss}), as well as degradation of the ferroelectric properties. During the measurement, the temperature was controlled by means of the Linkam THMS600 stage system.

3. Experimental results and discussion

The $\theta-2\theta$ X-ray images from the BNFNO/Pt/MgO heterostructure under study (Fig. 1) recorded only reflections from respective planes for the BNFNO, Pt layers and the MgO substrate. But, neither traces of the $BaFe_{12}O_{19}$ barium hexaferrite (whose lines were identified at the angles $2\theta \sim 32.09^\circ$ in [2]), nor any other impurity phases were found. The lines were analyzed to demonstrate that in our technological modes there is an oriented growth of the BNFNO crystals along a normal to a substrate surface. The lattice cell parameter of the BNFNO layer is equal to $c = 3.976 \pm 0.001$ Å, while for the Pt electrode it is equal to $c = 3.938 \pm 0.001$ Å. The obtained parameter of the BNFNO layer's lattice cell corresponds to quite large

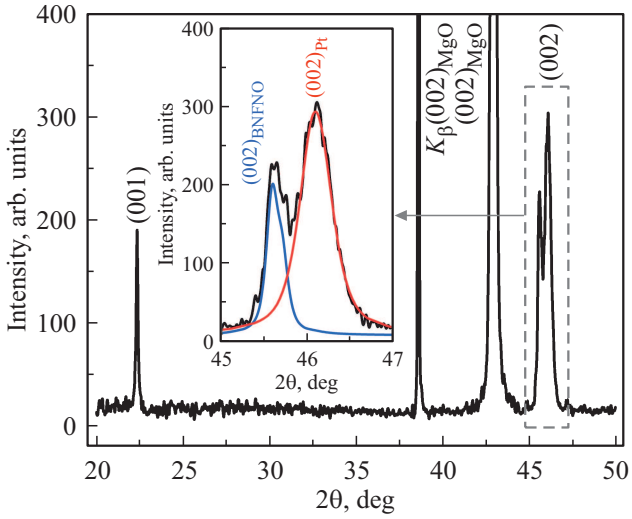

Figure 1. $\theta-2\theta$ X-ray image of the BNFNO/Pt/MgO film, the insert includes an enlarged area of reflections (002) of the BNFNO and Pt films.

tensile strain of the lattice cell of 1.35% in comparison with parameters of the bulk material ($c_{\text{bulk}} = 3.923$ Å; $a_{\text{bulk}} = 12.477$ Å). The $Ba_2LnFeNb_4O_{15}$ multiferroics have a polar state due to shifting of the cations Fe^{3+} and Nb^{5+} along the axis of the fourth order [6,7]. As it follows from the symmetry analysis, the ferroelectric polarization is in the same direction. It allowed us to study the dielectric (Fig. 2) and ferroelectric properties (Fig. 3) directly along the polar direction. The Pt/BNFNO/Pt condenser structures were formed for this. At the room temperature, the BNFNO film was characterized by average values $\varepsilon'/\varepsilon_0$ and dispersion (Fig. 2, *a*): at $f = 200$ Hz the value $\varepsilon'/\varepsilon_0$ was 1620, at $f = 200 \cdot 10^5$ Hz there is sharp decrease in the relative permittivity to 255, and at $f = 10^5-10^6$ Hz it is getting to a plateau. The dependences $\varepsilon''/\varepsilon_0(f)$ (Fig. 2, *a*) and $\mathrm{tg}\,\delta(f)$ (Fig. 2, *b*) show fuzzy maximums, but contribution by the two components is more clear on the curve $\mathrm{tg}\,\delta(f)$. The Cole–Cole diagram (Fig. 2, *d*) has a semi-circle arc formed, and the dispersion of the dielectric parameters is observed due to dielectric relaxation proceeding within this frequency range. As it is clear from the dependence $\gamma'(f)$ (Fig. 2, *c*), contribution of the through conductivity γ_{st} to the measured values $\varepsilon''/\varepsilon_0$ and $\mathrm{tg}\,\delta$ can be neglected in the range being analyzed. The experimental dependences of the Fig. 2, *a–d* are satisfactorily approximated by using the following relationship:

$$\varepsilon^* = \varepsilon' + i \cdot \varepsilon'' = \varepsilon_{\infty 1} + \frac{\varepsilon_{s1} - \varepsilon_{\infty 1}}{1 + (i \cdot f \cdot \tau_1)^{1-\alpha_1}} + \frac{\varepsilon_{s2} - \varepsilon_{s1}}{1 + (i \cdot f \cdot \tau_2)^{1-\alpha_2}}, \quad (1)$$

where α_1 and α_2 — coefficients characterizing relaxation time distributions (from 0 to 1), ε_{s1}, ε_{s2} and $\varepsilon_{\infty 1}$ — static and high-frequency permittivities; τ_1 and τ_2 — relaxation time.

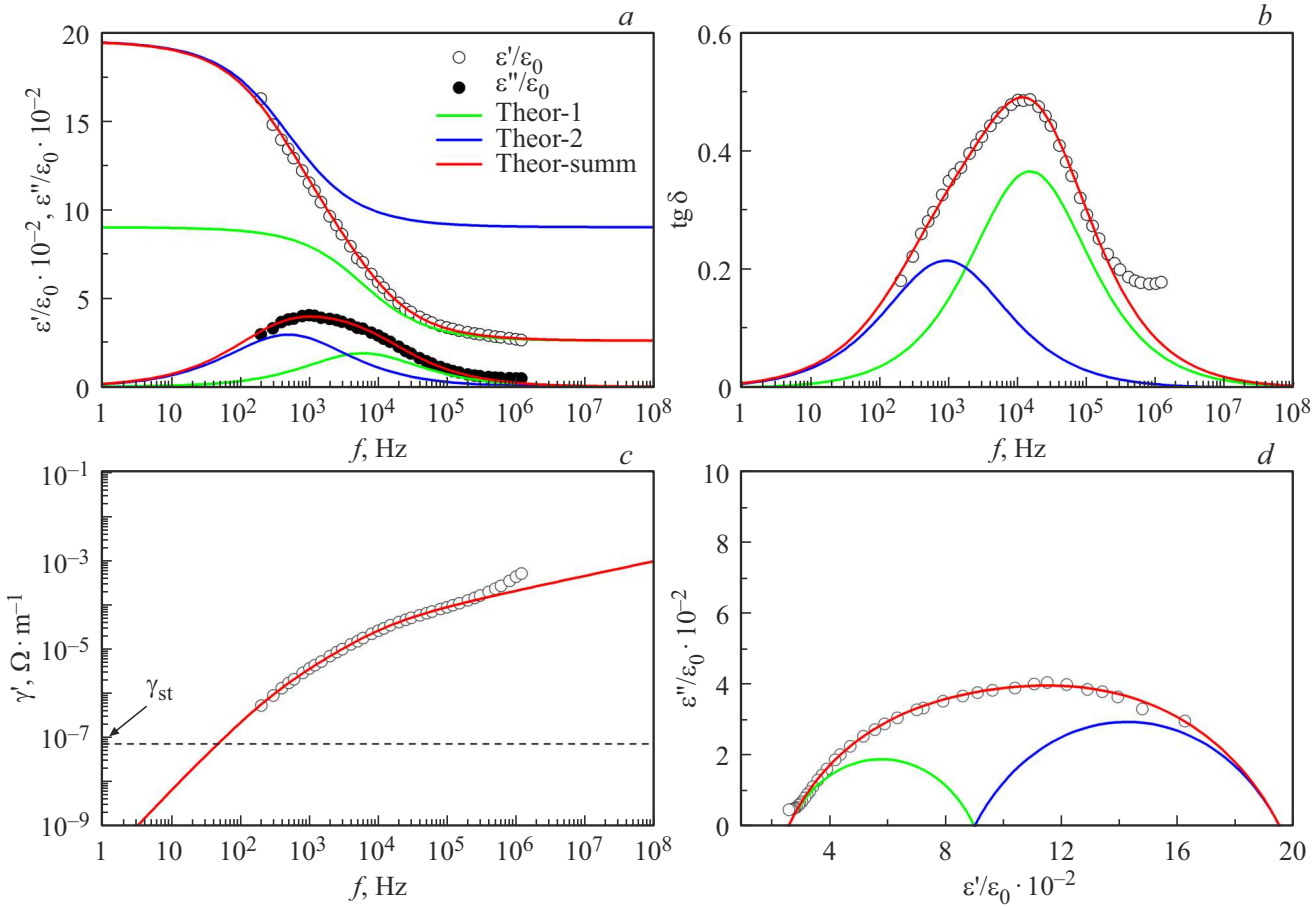

Figure 2. Dependences $\varepsilon'/\varepsilon_0(f)$, $\varepsilon''/\varepsilon_0(f)$ — (a), $\mathrm{tg}\,\delta(f)$ — (b), $\gamma'(f)$ — (c) and $\varepsilon''/\varepsilon_0(\varepsilon'/\varepsilon_0)$ — (d) for the Pt/BNFNO/Pt(001)/MgO(001) heterostructure have been measured at the room temperature within the frequency range $f = 200-1.2\cdot10^6$ Hz. The following parameters were used for approximation: $\varepsilon_{s2} = 1950$, $\varepsilon_{\infty2} = 900$, $\alpha_2 = 0.35$, $\tau_2 = 0.002$ s (the lines teor-1); $\varepsilon_{s1} = 900$, $\varepsilon_{\infty1} = 255$, $\alpha_1 = 0.32$, $\tau_1 = 0.00016$ s (the lines teor-2).

It is clear that the dielectric response of the BNFNO film is contributed by two processes, which are most probably non-Debye ones (as they are described by a model, which takes into account availability of the relaxation time distribution for each process). In [3], when studying the dielectric properties of the films $Ba_2LnFeNb_4O_{15}$ (Ln = La, Nd, Eu) within the temperature range of 80–420 K, the authors have noted two anomalies, one of which is correlated to a phase transition from a ferroelectric to paraelectric phase, while the other — to emerging effects of the Maxwell-Wagner (MW) polarization. Annealing of the films in oxygen led to almost no contribution by the MW polarization. Taking into account that in our case the ferroelectric phase in the BNFNO films is implemented at the room temperature (to be proven below), and that after the synthesis in the technological process the heterostructure cools down to the room temperature in the a pure oxygen atmosphere at the pressures of 0.5–0.6 T, then the found dielectric relaxation is due to the response of the ferroelectric subsystem of the film.

Measured loops of the BNFNO ferroelectric hysteresis are shown in the Fig. 3. The dependence $P(U)$ was typical for the ferroelectrics, but it was shifted to negative electric fields due to an internal field in the film. It leads to spontaneous „on-polarization“ of the films, which is directed from the substrate. The BNFNO ferroelectric parameters evaluated from the dependence $P(U)$ are given in the table. Taking into account of a shift of the loop and the film thickness, the residual polarization was $P_r = 4.08\,\mu\mathrm{C/cm^2}$, the coercive field was

Parameters of the BNFNO film

Cycle number	1	10^6	10^9
V_c^+, V	0.42	0.43	0.43
V_c^-, V	−1.03	−1.04	−1.02
P_r^+, μC/cm^2	5.26	5.34	5.14
P_r^-, μC/cm^2	−2.90	−2.97	−2.91
$P_{\max}^+$, μC/cm^2	12.24	12.23	12.22
$P_{\max}^-$, μC/cm^2	−12.24	−12.23	−12.22
W_{loss}, μJ/cm^2	25.27	25.8	25.28

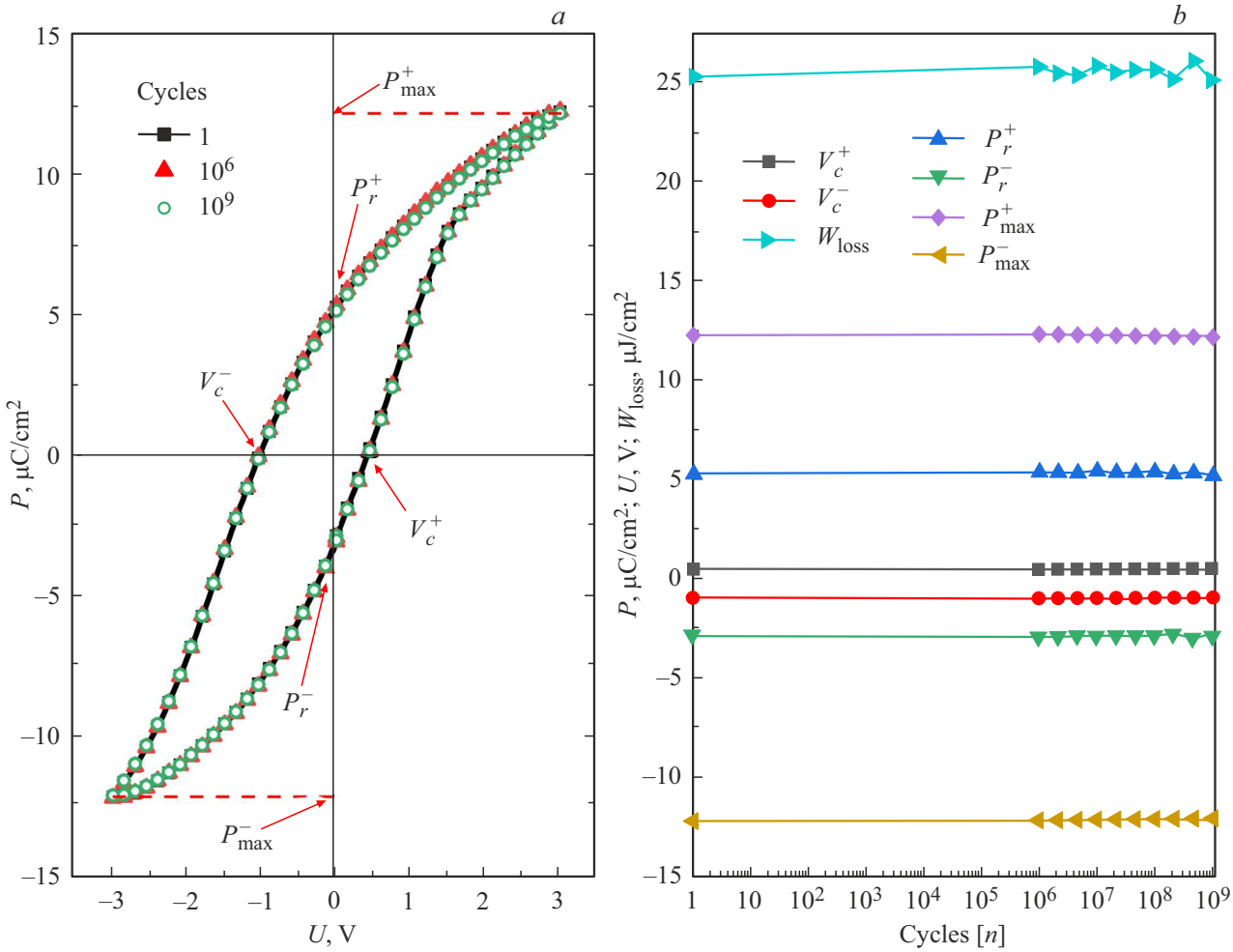

Figure 3. (a) dependence $P(U)$ of the Pt/BNFNO/Pt(001)/MgO(001) heterostructure at the room temperature at the frequency 180 Hz, (b) dependencies of polarization characteristics of the material on a number of the switching cycles.

$E_c = 17$ kV/cm, and the energy switching losses were $W_{\text{loss}} = 25.27\,\mu\text{J/cm}^2$. The coercive field, residual and full polarization recorded in our case were comparable to those for the BNFNO/Pt(111)/Si(001) c-oriented films [14] and exceeded those for BNFNO/Pt(001)/MgO(001) [15]. The analysis of the ferroelectric fatigue of the BNFNO film (Fig. 3, b) established that unlike [15], there was almost no record of degradation of their ferroelectric parameters up to the switching cycles 10^9 at the electric field frequency 10^6 Hz.

On the one hand, the results obtained mean that deformation of the lattice cell occurring in the BNFNO films (extension along the [001] direction) results in implementation of the ferroelectric phase even at the room temperature. On the other hand, they underline a significant impact of both a film production method, and process conditions on their phase composition and ferroelectric properties. Taking this into account, we have additionally studied the surface topography and the ferroelectric properties of the BNFNO films using PFM (Figures 4, 5). The BNFNO film surface (Fig. 4) is quite homogeneous, and there were clear crystallites of a various shape (from a round to trapezoidal shape), but their joint locations were predominantly flat. There was no inclusion of impurity phases, no pore, neither cavern. The mean-square roughness of the film surface was 5.7 nm. For quantitative estimation of a lateral size of the grains, we have used the autocorrelation function method [16] similar to [17]. The 2D-representation of the autocorrelation function, which was calculated in the analysis of the results of the BNFNO film surface studies, is given in the Fig. 4, b. The calculations showed that the average lateral size of the crystallites was ~ 145 nm (Fig. 4, b).

The vertical piezoresponse for the BNFNO film's entire area under study has a negative sign (Fig. 5, a), which confirms a direction of a polarization vector projection from the substrate to the film, thereby correlating to results of the study of the dielectric hysteresis loops (Fig. 3). The histogram of the piezoresponse lateral signal distribution $\sim$ is symmetrical in relation to zero, and at the same time a maximum number of pixels is on the histogram with a zero signal. That is, the BNFNO film polarization is mainly

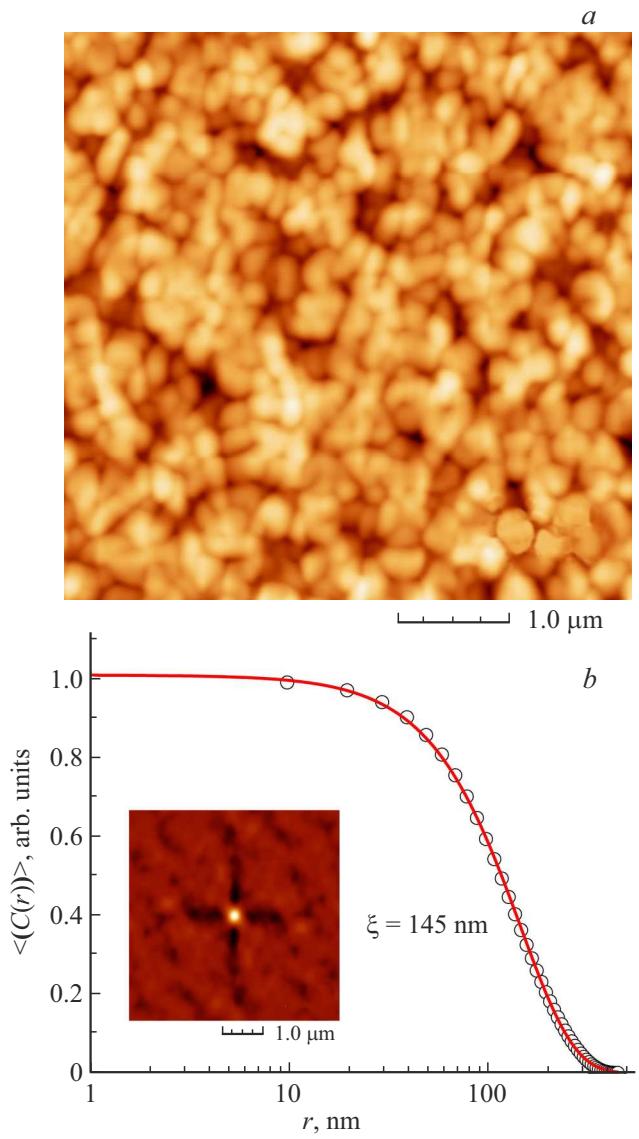

Figure 4. Topography of the BNFNO film (*a*), 2*D*-representation of the autocorrelation function and curve of the radially averaged values of the mean-sized crystallites (*b*).

along the axis c, while misorientation of the polarization vector is quite small in the lateral plane. This supports the assumption that the internal field and „on-polarization" occurs in the thin BNFNO films as it is affected by the substrate in the increase in the two-dimensional mechanical stresses [18]. The joint analysis of images of the relief, the vertical and lateral piezoresponse showed that we did not reveal any signs of inclusions of non-ferroelectric phases, for example —of barium hexaferrite, which were reported in [3,4,16]. It is correlated to the data of X-ray diffraction analysis.

Taking into account the above results, the Kelvin-mode routine has been taken to study the relaxation of the polarized areas, which are pre-formed in the PFM mode with the voltage of ±10 V (Fig. 6, *a*–*b*): a light rectangle — as resulted from +10 V applied to the cantilever, while the dark one — polarization at −10 V. The Fig. 6, *c* shows the surface potential signal profiles in 23 (the curve *1*) and 136 min (the curve *2*) after the polarization, as obtained by the surface potential signal data. There is evident

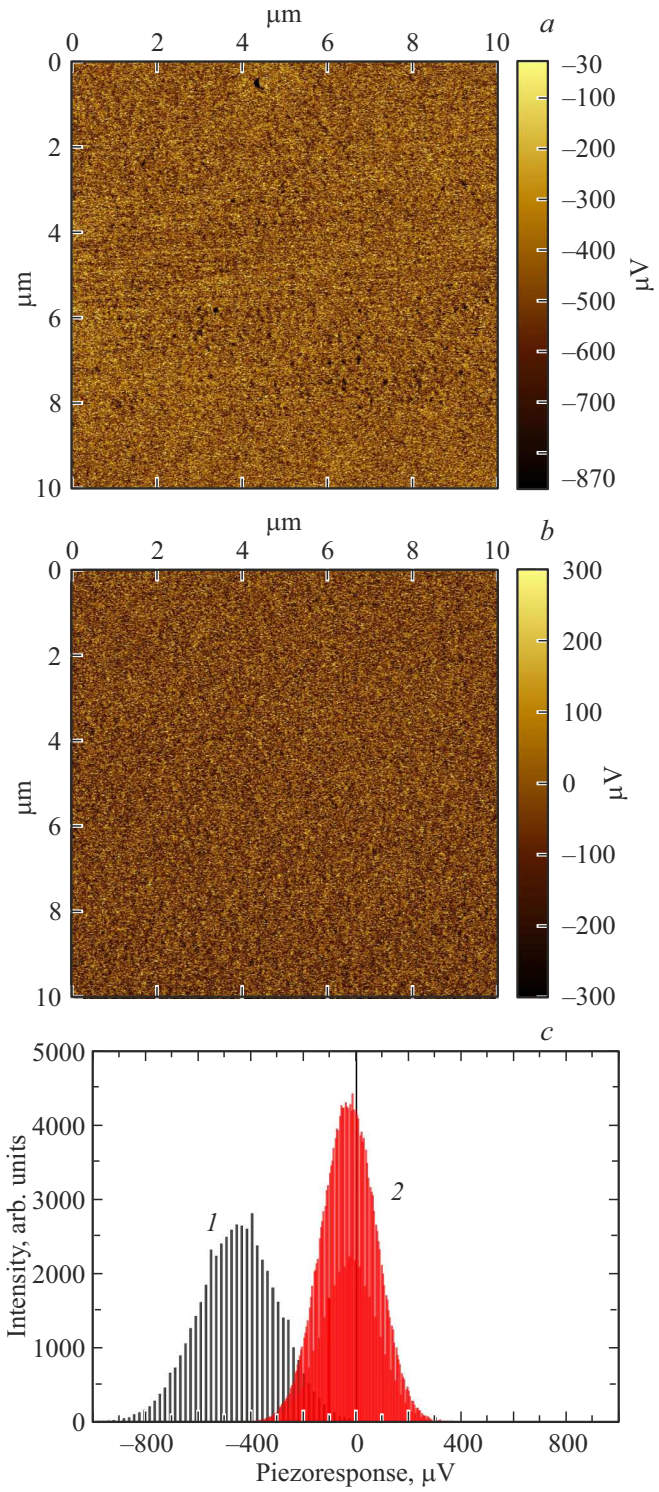

Figure 5. The vertical (*a*) and lateral (*b*) signal of the piezoresponse, *c* — piezoresponse signal distribution histograms: *1* — vertical, *2* — lateral.

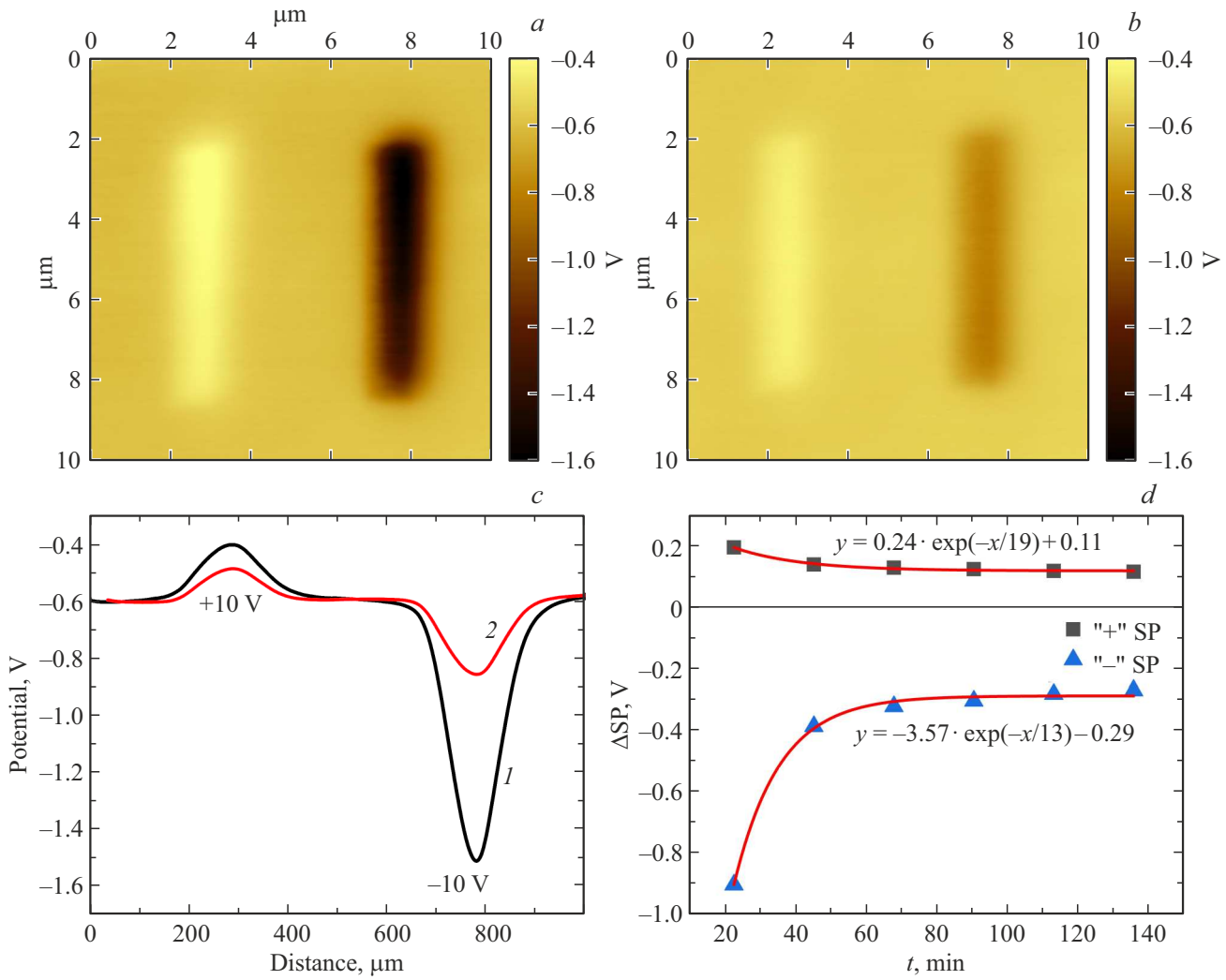

Figure 6. Signal of the surface potential of the polarized BNFNO film, as received in 23 (*a*) and 136 min (*b*) after polarization with the constant voltage ±10 V, *c* — surface potential signal profiles in 23 (the curve *1*) and 136 min (the curve *2*) after polarization, *d* — time dependence of the signal ΔSP.

asymmetry of the signal intensity in the areas polarized with the constant voltage +10 V and −10 V. The Fig. 6, *d* shows relaxation dependences of the signal ΔSP for the positively and negatively polarized areas. The amplitude values of the polarized areas for ±10 V have been calculated in the Gwyddion software by approximation of the obtained profiles with an amplitude version of the Gaussian function. That is why the signal values ΔSP (Fig. 6, *d*) for the area polarized at +10 V — positive, and for −10 V — negative, although the whole level of the surface potential signal — negative (Fig. 6, *c*). It is clear that the internal field in the films causes faster relaxation of the negatively charged area of the film ($t = 13$ min) in comparison of the positively charged one ($t = 19$ min). However, the residual „on-polarization" remains for a long time in both the cases. Presently, it is not ascertained whether the BNFNO films belong to relaxors or traditional ferroelectrics. However, preliminary studies have revealed signs of polarization at the temperature above 100°C, too.

4. Conclusions

1. The $Ba_2NdFeNb_4O_{15}$ nanosized films are grown on the Pt(001)/MgO(001) substrate by the HF-cathode sputtering method in the O_2 atmosphere. As per the data of the X-ray diffraction analysis and scanning probe microscopy, the films are *c*-oriented, single-phased, impurity-free and characterized by high homogeneity and low roughness of the surface (5.7 nm) with a lateral size of the crystallites ∼ 145 nm (the calculations were carried out by the autocorrelation function method).

2. The deformation of the lattice cell in the $Ba_2NdFeNb_4O_{15}$ film along the polar axis was 1.35% of that of the bulk material, thereby resulting in the ferroelectric properties even at the room temperature — the values

of the residual polarization and the coercive field were $4.08\,\mu C/cm^2$ and 17 kV/cm, respectively. There was almost no degradation of the ferroelectric parameters up to the billion switching cycles.

3. The analysis of the change of $\varepsilon^*/\varepsilon_0$ of the BNFNO film within the frequency range of $200-1.2\cdot10^6$ Hz at the room temperature has shown that the dielectric response of the material is contributed by the two relaxation processes, which cause a recorded dielectric dispersion.

4. The studies of the vertical and lateral signal of the BNFNO film piezoresponse demonstrated that the polarization therein is mainly along the axis *c*, while misorientation of the polarization vector is quite small in the lateral plane.

5. The results obtained are to be included in the synthesis, research and development of functional elements based on nanosized films of the BNFNO multiferroic.

Funding

The study has been carried out at the cost of the Russian Scientific Foundation's grant No. 21-72-10180.

Conflict of interest

The authors declare that they have no conflict of interest.

References

[1] Yu.S. Kuz'minov. Ferroelectric crystals to control laser radiation. Nauka, M. (1982). 400 p.
[2] T. Hajlaoui, C. Harnagea, A. Pignolet. Mater. Lett. **198**, 136 (2017).
[3] R. Bodeux, D. Michau, M. Josse, M. Maglione. Solid State Sci. **38**, 112 (2014).
[4] M. Josse, O. Bidault, F. Roulland, E. Castel, A. Simon, D. Michau, R. Von der Mühll, O. Nguyen, M. Maglione. Solid State Sci. **11**, *6*, 1118 (2009).
[5] H. Wu, A. Tatarenko, M.I. Bichurin, Y. Wang. Nano Energy **83**, 105777 (2021).
[6] M. Albino, P. Veber, S. Pechev, C. Labrugere, M. Velazquez, M. Maglione, M. Josse. Cryst. Growth Des. **14**, *2*, 500 (2014).
[7] E. Castel, P. Veber, M. Albino, M. Vela′zquez, S. Pechev, D. Denux, J.P. Chaminade, M. Maglione, M. Josse. J. Cryst. Growth **340**, 156 (2012).
[8] Ferroelectric physics. Modern view / Ed. by K.M. Rabe, Ch.G. Ana, Zh.-M. Triskona. Translated from English BINOM. Laboratoriya znanij, M. (2011). 440 p.
[9] V.M. Mukhortov, Yu.I. Yuzyuk. Heterostructures based on nanosized ferroelectric films: production, properties and application. SSC RAS, Rostov n/D. (2008). 224 p.
[10] A.V. Pavlenko, D.V. Stryukov, L.I. Ivleva, A.P. Kovtun, K.M. Zhidel', P.A. Lykov. Physics of the Solid State **63**, *2*, 250 (2021).
[11] A.V. Pavlenko, I.N. Zakharchenko, Yu.A. Kudryavtsev, L.I. Kiseleva, S.Kh. Alikhadzhiev. Neorgan. materialy **56**, *11*, 1252 (2020) (in Russian).
[12] V.M. Mukhortov, Yu.I. Golovko, A.V. Pavlenko, D.V. Stryukov, S.V. Biryukov, A.P. Kovtun, S.P. Zinchenko. Physics of the Solid State **60**, *9*, 1741, (2018).
[13] D.V. Stryukov, A.V. Pavlenko, L.I. Kiseleva, G.N. Tolmachev. In: PHENMA 2021: Physics and Mechanics of New Materials and Their Applications. Springer Proceedings in Materials/ Eds I.A. Parinov, S.-H. Chang, Y.-H. Kim, N.-A. Noda. Springer, Cham. (2021) P. 53.
[14] T. Hajlaoui, C. Harnagea, D. Michau, M. Josse, A. Pignolet. J. Alloys Comp. **711**, 480 (2017).
[15] T. Hajlaoui, C. Chabanier, C. Harnagea, A. Pignolet. Scripta Mater. **136**, 1 (2017).
[16] R.C. Munoz, G. Vidal, M. Mulsow, J.G. Lisoni, C. Arenas, A. Concha, R. Esparza. Phys. Rev. B **62**, *7*, 4686 (2000).
[17] A.V. Pavlenko, D.A. Kiselev, Ya.Yu. Matyash. Physics of the Solid State **63**, *6*, 776 (2021).
[18] A.G. Kanareikin, E.Yu. Kaptelov, S.V. Senkevich, I.P. Pronin, A.Yu. Sergienko, O.N. Sergeeva. Physics of the Solid State **58**, *11*, 2242 (2016).